International Journal of Applied Engineering Research ISSN 0973-4562 Volume 12, Number 17 (2017) pp. 6693-6698

The Validity of the Diagnosis of Plant Leaf Infections Using Non-Destructive Optical Inspection Technique and Depth-Scan Signal Analysis

Ruchire Eranga Wijesinghe[1], Seung-Yeol Lee[2], Hee-Young Jung[2,*], Mansik Jeon[1,*], and Jeehyun Kim[1]

[1]School of Electronics Engineering, College of Information Technology, Engineering, Kyungpook National University, Daegu 41566, Republic of Korea.

[2]School of Applied Biosciences, Kyungpook National University, Daegu 41566, Republic of Korea.

Abstract

The applicability of non-destructive optical imaging technique for the diagnosis of infected leaf materials was investigated along with a depth-scan (amplitude depth profile) signal analysis. The experimented plant leaf specimens were collected from persimmon plantations and the specimens were categorized into three groups: healthy leaf specimens, infected leaf specimens, and apparently healthy leaf specimens collected from infected trees. The non-destructive diagnosis was performed using 840 nm spectral domain optical coherence tomography (SD-OCT) system. The obtained OCT results confirmed that the proposed method is capable of identifying morphological differences between healthy specimens from infected specimens and partially infected specimens. Therefore, this method has the potential to generate significant cost savings in the field of agriculture through the accurate and rapid analysis of leaf infections at an initial stage.

Keywords: Optical coherence tomography, SD-OCT, Leaf infections.

INTRODUCTION

Persimmon is mainly cultivated in East Asian countries, such as Korea, Japan and China. Various plant pathogenic diseases can infect on persimmon, and among them, circular leaf spot is the most destructive disease in persimmon cultivation [1]. This disease makes discoloration and defoliation on diseased leaves, premature fruit maturation and abscission, which lead to an enormous economic loss on persimmon orchards [2, 3]. Hence, early diagnosis is essential to control this disease due to the long incubation period compared with other diseases [4]. The existing agricultural inspection techniques for plant diseases are carried out visually and using costly conventional optical methods, such as light microscopy, scanning electron microscopy, magnetic resonance imaging (MRI), and transmission electron microscopy (TEM) [5-12]. However, the potential applicability of these methods has been limited by factors due to low resolution, limited penetration, and long acquisition time. Moreover, the interest towards non-destructive techniques has been increased rapidly due to the requirement of time consuming precise sectioning techniques.

To compensate for these major limitations of the aforementioned techniques, non-destructive, high-resolution, and high sensitive imaging technique called optical coherence tomography (OCT) was introduced for biological imaging, which is capable of providing real-time cross-sectional and three-dimensional images [13-15]. Ophthalmology was the fundamental and frequent application of OCT [16, 17], then later extensively applied in dentistry [18, 19], otolaryngology [20, 21], and for the inspection of industrial defects [22-24]. Owing to various technical developments of OCT, the interest has been grown increasingly in the field of agriculture during past decade [25, 26]. Furthermore, OCT was implemented for number of applications including assessment of horticulture products, such as microstructural analysis of kiwi and apple peels to introduce three dimensional image protocols [27, 28]. The diagnosis of various infections in melon seeds, cucumber seeds, apple leaves, and orchids were quantitatively and qualitatively analyzed to limit the spread of diseases in plantations [29-35]. Apart from the OCT based plant disease diagnosis protocols, an additional OCT-based quantification study was performed by our group to determine the seed germination rate [36].

The main objective of this study is to introduce a plant leaf disease diagnosis protocol by examining variations in the internal thickness of leaf specimens. To explore the aforementioned morphological differences of leaf specimens at an initial stage, we utilized SD-OCT optical imaging modality, which provides precise cross-sectional images with a high-resolution. OCT image based depth-scan (amplitude depth profile) signal analysis was performed to evaluate the thickness difference between leaf layers. The obtained results verified that the extended OCT application has the capability to visualize and characterize internal microstructural changes of leaf specimens that are useful in agriculture for the initial diagnosis.

MATERIALS AND METHOD

The plant materials

The experimented leaf specimens were collected from persimmon orchards in Sangju, Korea. To maintain the biological nature of specimens, the experiment was performed within 2 hours of sample collection. The specimens were randomly collected from healthy and infected trees to investigate morphological variations. All these plant materials were inspected using a customized spectral domain OCT system (SD-OCT).

OCT based optical screening system

A spectrometer-based, customized, compact spectral domain OCT (SD-OCT) system was designed as the OCT engine of the imaging modality. The designed schematic diagram of the system is illustrated in Figure 1. The broadband light source was a super-luminescent diode (EXS210068-01, Exalos, Switzerland) with a center wavelength of 840 nm and bandwidth of 55 nm. The incident beam of the light source was split evenly, using a 50:50 optical fiber coupler, into the reference arm and the sample arm. Optical scanning mirrors (GVS002, Thorlabs, USA) were used in the sample arm for transverse scanning. The reflected beams from the sample arm and the reference arm give rise to an interference pattern when the light beams from both arms have travelled same optical path lengths, which is less than the coherence length of the broadband laser source. An optical spectrometer containing a 2048-pixel line scan camera (spL2048-140km, Basler, Germany) was used to detect the generated interference signal pattern and for image acquisition, and a transmission-type diffraction grating (spatial frequency 1800 lpmm, Wasatch Photonics, USA) with nominal diffraction angle of 46.05°, was adapted to diffract the light into components at the detection end. The system has 8 μm and 13 μm axial and lateral resolutions when measured in air [16].

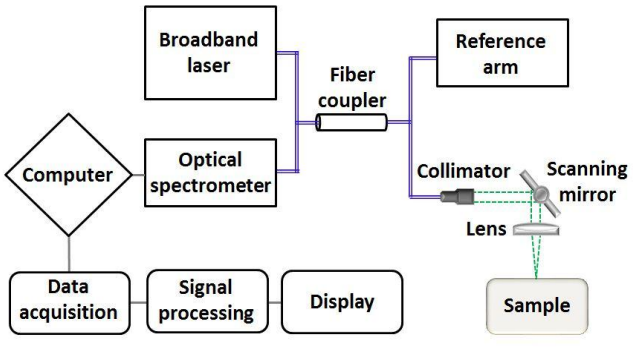

Figure 1: The schematic diagram of the non-destructive optical imaging technique (SD-OCT).

Real-time image processing algorithm

The real-time computing for image processing technique was implemented to acquire, process, and display the data. High-speed data processing was performed using computer unified device architecture (CUDA) with a GTX480 NVIDIA graphics-processing unit (GPU) [23]. The frame rate of the system was significantly increased from 10 frames/s to 60 frames/s with the image size of 2048 × 500 pixels. The subtraction of background noise, zero padding, k-domain linearization, fast Fourier transform (FFT), and log scaling are included in GPU data processing. The fast Fourier transformation (FFT) was implemented by CUFFT using GPU based CUDA technique. The detected spectrum as a function of wavenumber, k, is given by

$$I(k) = \left|E_{ra}(k)\right|^2 + 2\,\mathrm{Re}\{\mathrm{E}^*_{ra}(k) * \mathrm{E}_{sa}(k)\} + \left|E_{sa}(k)\right|^2 \quad (1)$$

Where, E_{ra} is the reference arm field and E_{sa} is the sample arm field, including delay and attenuation. The interference term $I_{int}(k)$, contains the image information and is the sum of fringes generated by the interference of light reflected from index variations within an object with the light reflected from reference arm.

$$I_{\mathrm{int}}(k) = 2\,\mathrm{Re}[E^*_{ra}(k) * E_{sa}(k)], \quad (2)$$

$$= 2\,\mathrm{Re}\{\sum_n \sqrt{I_n(k) I_{ra}(k)}\exp[i(kz_n + \varphi(k, z_n))]\} \quad (3)$$

Where I_n is the intensity of light reflected from the nth layer of the sample, I_{ra} is the intensity of light reflected from the reference arm. Z_n is the depth of the nth reflection and $\varphi(k, z_n)$ is a general phase term that includes dispersive effects. The calibration of wavenumber-domain linearization was used to remove the non-linearity in the raw signal [37].

RESULTS AND DISCUSSION

Randomly chosen six positions closed to the middle vein region from each leaf specimen were diagnosed during the experiment. The topographical images of the leaf specimens (Fig. 2(a, b, and c)) are shown along with the representative two-dimensional (2D) OCT images (Fig. 2(d, e, and f)). Clearly identifiable topographical differences between infected and healthy leaf specimens were visualized. However, no topographical difference was identified between healthy leaves and apparently healthy but infected leaf specimens. The acquired corresponding two dimensional OCT images confirm a clear difference in thickness between the first and second top layers. Although the physical appearance of leaf specimens in the topography looks similar, the OCT cross-sectional images of healthy leaves from healthy trees, and healthy leaves from infected trees show notable morphological differences, which confirms that OCT is capable of identifying symptoms at an initial stage.

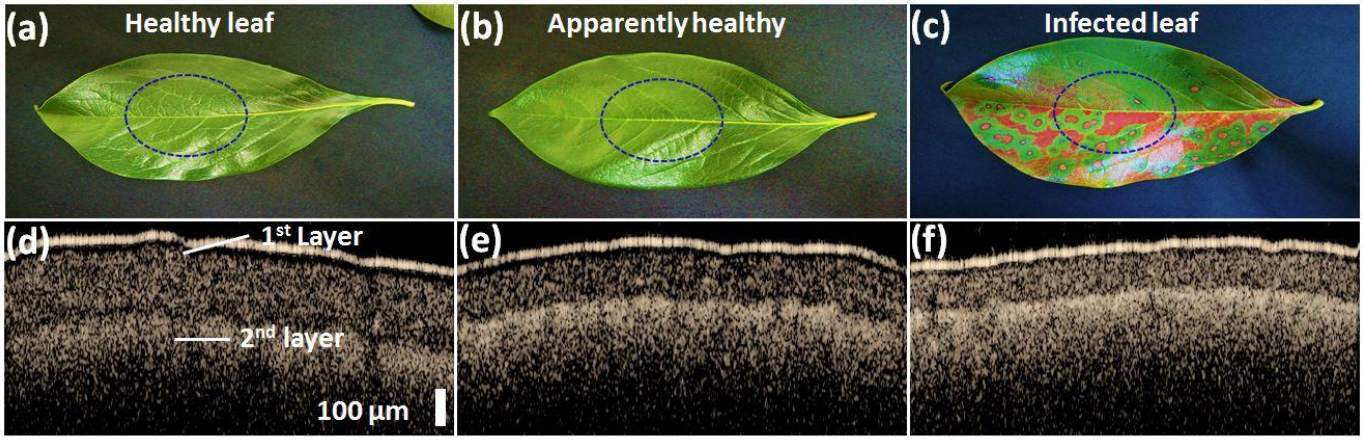

Figure 2: The external appearance of the specimens along with the OCT cross-sectional images. (a) Photograph of a healthy leaf specimen. (b) Photograph of an apparently healthy but infected leaf specimen. (c) Photograph of an infected leaf specimen. (d, e, and f): The corresponding OCT images.

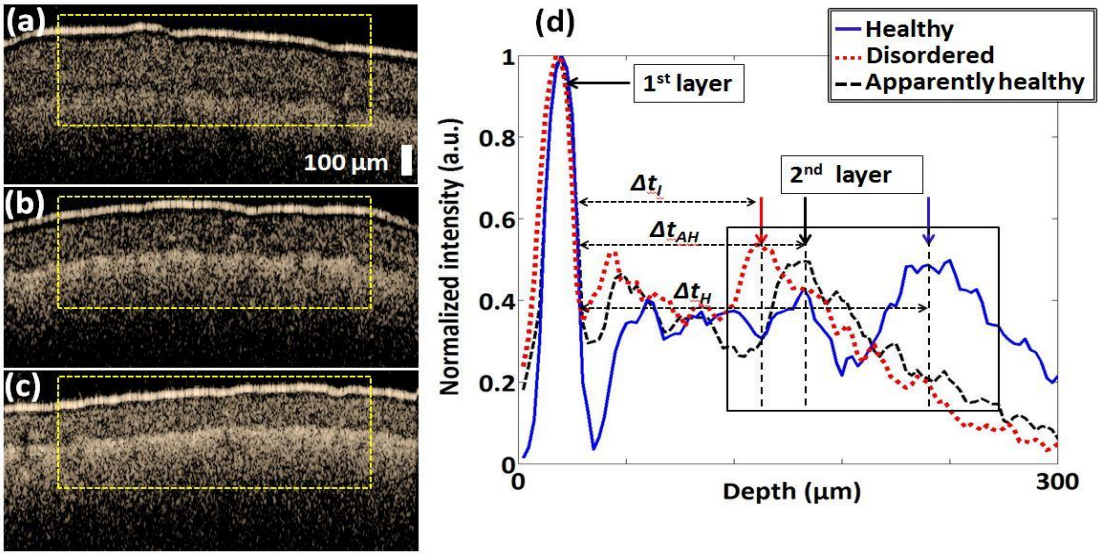

Figure 3: The A-scan depth profiles of healthy, apparently healthy, and infected leaf specimens and corresponding layer information. (a, b, and c): 2D OCT images of healthy leaf specimen, an apparently healthy but infected leaf specimen, and infected leaf specimen. In Fig 3(d), Blue solid curve: A-scan depth profile of healthy specimens, red dotted curve: A-scan depth profile of infected or disordered specimens, black dashed curve: A-scan depth profile of apparently healthy specimens, and yellow dashed square region depicts the selected region of interest for the intensity signals.

The depth scan OCT signals based A-scan profiles (amplitude depth profiles) were analyzed to detect the layer thickness reduction between leaf layers. The A-scans obtained from the depth direction are illustrated in Figure 3(d). The peak information shown in the A-scan profile depicts internal layers localized at different depth levels. For brevity, only the peak OCT signals will be described. The two peaks with higher intensities of each depth profile correspond to the two visible layers (1st and 2nd) in each OCT image, and Δt (Δt_H, Δt_{AH}, and Δt_I) represents the difference in thickness between the top two layers. Here, the Δt magnitude seen in Fig. 3(d) was reduced and moved towards the 1st peak as a result of infection. The aforementioned reduction in thickness is considered to be the main initial symptom of the disease, and it is essential to identify the difference in thickness (Δt) between leaf layers at an earlier disease stage in order to determine the physical status of the leaf sample. The average peak for apparently healthy leaf specimens from infected trees was located between healthy and infected peaks, which confirm the ability of the developed disease inspection protocol based on OCT to identify the physical state of the leaf specimens at an advanced stage of infection.

Table 1: The average, standard deviation (STD), minimum, and maximum thicknesses of three leaf categories.

Leaf category	Avg. (μm)	STD (μm)	Min. (μm)	Max. (μm)
Healthy	248.51	8.52	223.4	255.21
Apparently healthy	178.32	1.93	160.36	187.29
Infected	120.82	1.73	48.25	124.66

To measure the leaf layer thickness of the experimented three leaf categories, a post-acquisition process was performed for all the acquired 2D-OCT images. The thickness between 1st and 2nd layers was measured and illustrated in table 1 along with minimum and maximum measurements. The thickness was measured by considering the distance between averaged A-scan peak information. To enhance the accuracy of leaf thickness measurements, six different positions were selected and acquired 2D-OCT images from each leaf specimen. The quantitative measurements revealed a clear correlation between the cross-sectional images, which confirms the feasibility and efficacy of the developed diagnostic modality. Moreover, the obtained numerical readings can be considered as powerful threshold values for the identification of the physical status of the leaf (healthy or infected) at advanced stages of these diseases.

CONCLUSION

Morphological and quantitative analyses have advantages in agriculture for diagnostic evaluations of plant related diseases. Thus, we implemented a non-destructive optical inspection technique (SD-OCT) based depth-scan (amplitude depth profile) signal analysis method to investigate the capability of OCT to identify the leaf infections at an initial stage. Especially in the field of agriculture, most disease inspection procedures are destructive and time consuming. Moreover, from the agricultural point of view, no topographical differences can be observed between healthy samples and newly infected (initial stage of an infection) samples. Hence, existing agricultural inspection methods have various limitations for identifying newly infected samples. To overcome these limitations, we performed various OCT-based agricultural experiments to confirm that OCT can be applied to reliably identify healthy, newly-infected, and infected plant materials. The obtained cross-sectional results and depth direction signals clearly indicate that the OCT method is sufficiently capable of identifying plant material infections at an initial stage, which are hard to be distinguished with visual inspection. Furthermore, the proposed method may be used to control the spread of various plant related diseases in the field of agriculture.

ACKNOWLEDGEMENT

This work was supported by Korea Institute of Planning and Evaluation for Technology in Food, Agriculture, Forestry and Fisheries (IPET) through Advanced Production Technology Development Program, funded by Ministry of Agriculture, Food and Rural Affairs (MAFRA) (No. 314031-3)

REFERENCES

[1] M. Berbegal, A. Pérez-Sierra, J. Armengol, C. Park, and J. García-Jiménez, "First report of circular leaf spot of persimmon caused by Mycosphaerella nawae in Spain," *Plant Disease*, vol. 94, pp. 374-374, 2010.

[2] J.-H. Kwon and C.-S. Park, "Ecology of disease outbreak of circular leaf spot of persimmon and inoculum dynamics of Mycosphaerella nawae," *Research in Plant Disease*, vol. 10, pp. 209-216, 2004.

[3] M. Berbegal, B. Mora-Sala, and J. García-Jiménez, "A nested-polymerase chain reaction protocol for the detection of Mycosphaerella nawae in persimmon," *European journal of plant pathology*, vol. 137, pp. 273-281, 2013.

[4] A. Vicent, D. D. Bassimba, C. Hinarejos, and J. L. Mira, "Inoculum and disease dynamics of circular leaf spot of persimmon caused by Mycosphaerella nawae under semi-arid conditions," *European journal of plant pathology*, vol. 134, pp. 289-299, 2012.

[5] A. Rizzolo, M. Vanoli, G. Cortellino, L. Spinelli, D. Contini, E. Herremans, E. Bongaers, A. Nemeth, M. Leitner, and P. Verboven, "Characterizing the tissue of apple air-dried and osmo-air-dried rings by X-CT and OCT and relationship with ring crispness and fruit maturity at harvest measured by TRS," *Innovative Food Science & Emerging Technologies*, vol. 24, pp. 121-130, 2014.

[6] J. F. Cajuste, F. J. García-Breijo, J. Reig-Armiñana, and M. T. Lafuente, "Ultrastructural and histochemical analysis reveals ethylene-induced responses underlying reduced peel collapse in detached citrus fruit," *Microscopy Research and Technique*, vol. 74, pp. 970-979, 2011.

[7] S. Freeman, T. Katan, and E. Shabi, "Characterization of Colletotrichum species responsible for anthracnose diseases of various fruits," *Plant disease*, vol. 82, pp. 596-605, 1998.

[8] M. A. Urban, R. S. Barclay, M. Sivaguru, and S. W. Punyasena, "Cuticle and subsurface ornamentation of

intact plant leaf epidermis under confocal and superresolution microscopy," *Microscopy Research and Technique*, 2016.

[9] P. Barreiro, C. Zheng, D.-W. Sun, N. Hernández-Sánchez, J. Perez-Sanchez, and J. Ruiz-Cabello, "Non-destructive seed detection in mandarins: comparison of automatic threshold methods in FLASH and COMSPIRA MRIs," *Postharvest Biology and Technology*, vol. 47, pp. 189-198, 2008.

[10] S. Jahnke, M. I. Menzel, D. Van Dusschoten, G. W. Roeb, J. Bühler, S. Minwuyelet, P. Blümler, V. M. Temperton, T. Hombach, and M. Streun, "Combined MRI–PET dissects dynamic changes in plant structures and functions," *The Plant Journal*, vol. 59, pp. 634-644, 2009.

[11] M. Shahin, E. Tollner, R. McClendon, and H. Arabnia, "Apple classification based on surface bruises using image processing and neural networks," *Transactions of the ASAE*, vol. 45, p. 1619, 2002.

[12] G. Batten, "Plant analysis using near infrared reflectance spectroscopy: the potential and the limitations," *Animal Production Science*, vol. 38, pp. 697-706, 1998.

[13] A. Fercher and C. Hitzenberger, "Optical coherence tomography," *Progress in optics*, vol. 44, pp. 215-302, 2002.

[14] J. G. Fujimoto, "Optical coherence tomography," *Comptes Rendus de l'Académie des Sciences-Series IV-Physics*, vol. 2, pp. 1099-1111, 2001.

[15] A. G. Podoleanu, "Optical coherence tomography," *Journal of Microscopy*, vol. 247, pp. 209-219, 2012.

[16] R. E. Wijesinghe, K. Park, P. Kim, J. Oh, S.-W. Kim, K. Kim, B.-M. Kim, M. Jeon, and J. Kim, "Optically deviated focusing method based high-speed SD-OCT for in vivo retinal clinical applications," *Optical Review*, pp. 1-9, 2015.

[17] M. F. Shirazi, R. E. Wijesinghe, N. K. Ravichandran, P. Kim, M. Jeon, and J. Kim, "Dual-path handheld system for cornea and retina imaging using optical coherence tomography," *Optical Review*, pp. 1-7, 2016.

[18] D. Fried, J. Xie, S. Shafi, J. D. Featherstone, T. M. Breunig, and C. Le, "Imaging caries lesions and lesion progression with polarization sensitive optical coherence tomography," *Journal of biomedical optics*, vol. 7, pp. 618-627, 2002.

[19] R. E. Wijesinghe, N. H. Cho, K. Park, M. Jeon, and J. Kim, "Bio-Photonic Detection and Quantitative Evaluation Method for the Progression of Dental Caries Using Optical Frequency-Domain Imaging Method," *Sensors*, vol. 16, p. 2076, 2016.

[20] N. H. Cho, J. W. Lee, J.-h. Cho, J. Kim, J. H. Jang, and W. Jung, "Evaluation of the usefulness of three-dimensional optical coherence tomography in a guinea pig model of endolymphatic hydrops induced by surgical obliteration of the endolymphatic duct," *Journal of biomedical optics*, vol. 20, pp. 036009-036009, 2015.

[21] J. Lee, K. Kim, R. E. Wijesinghe, D. Jeon, S. H. Lee, M. Jeon, and J. H. Jang, "Decalcification using ethylenediaminetetraacetic acid for clear microstructure imaging of cochlea through optical coherence tomography," *Journal of biomedical optics*, vol. 21, pp. 081204-081204, 2016.

[22] N. H. Cho, K. Park, J.-Y. Kim, Y. Jung, and J. Kim, "Quantitative assessment of touch-screen panel by nondestructive inspection with three-dimensional real-time display optical coherence tomography," *Optics and Lasers in Engineering*, vol. 68, pp. 50-57, 2015.

[23] M. F. Shirazi, K. Park, R. E. Wijesinghe, H. Jeong, S. Han, P. Kim, M. Jeon, and J. Kim, "Fast industrial inspection of optical thin film using optical coherence tomography," *Sensors*, vol. 16, p. 1598, 2016.

[24] R. E. Wijesinghe, K. Park, Y. Jung, P. Kim, M. Jeon, and J. Kim, "Industrial resin inspection for display production using automated fluid-inspection based on multimodal optical detection techniques," *Optics and Lasers in Engineering*, vol. 96, pp. 75-82, 2017.

[25] R. E. Wijesinghe, S.-Y. Lee, N. K. Ravichandran, S. Han, H. Jeong, Y. Han, H.-Y. Jung, P. Kim, M. Jeon, and J. Kim, "Optical coherence tomography-integrated, wearable (backpack-type), compact diagnostic imaging modality for in situ leaf quality assessment," *Applied Optics*, vol. 56, pp. D108-D114, 2017.

[26] N. K. Ravichandran, R. E. Wijesinghe, M. F. Shirazi, K. Park, M. Jeon, W. Jung, and J. Kim, "Depth enhancement in spectral domain optical coherence tomography using bidirectional imaging modality with a single spectrometer," *Journal of biomedical optics*, vol. 21, pp. 076005-076005, 2016.

[27] P. Verboven, A. Nemeth, M. K. Abera, E. Bongaers, D. Daelemans, P. Estrade, E. Herremans, M. Hertog, W. Saeys, and E. Vanstreels, "Optical coherence tomography visualizes microstructure of apple peel," *Postharvest Biology and Technology*, vol. 78, pp. 123-132, 2013.

[28] M. Li, P. Verboven, A. Buchsbaum, D. Cantre, B. Nicolai, J. Heyes, A. Mowat, and A. East, "Characterising kiwifruit (Actinidia sp.) near skin cellular structures using optical coherence tomography," *Postharvest Biology and Technology*, vol. 110, pp. 247-256, 2015.

[29] S.-Y. Lee, C. Lee, J. Kim, and H.-Y. Jung, "Application of optical coherence tomography to detect Cucumber green mottle mosaic virus (CGMMV) infected cucumber seed," *Horticulture, Environment, and Biotechnology*, vol. 53, pp. 428-433, 2012.

[30] C. Lee, S.-Y. Lee, J.-Y. Kim, H.-Y. Jung, and J. Kim, "Optical sensing method for screening disease in melon seeds by using optical coherence tomography," *Sensors*, vol. 11, pp. 9467-9477, 2011.

[31] C.-H. Lee, S.-Y. Lee, H.-Y. Jung, and J.-H. Kim, "The application of optical coherence tomography in the diagnosis of Marssonina blotch in apple leaves," *Journal of the Optical Society of Korea*, vol. 16, pp. 133-140, 2012.

[32] R. E. Wijesinghe, S.-Y. Lee, P. Kim, H.-Y. Jung, M. Jeon, and J. Kim, "Optical Inspection and Morphological Analysis of Diospyros kaki Plant Leaves for the Detection of Circular Leaf Spot Disease," *Sensors*, vol. 16, p. 1282, 2016.

[33] T. H. Chow, K. M. Tan, B. K. Ng, S. G. Razul, C. M. Tay, T. F. Chia, and W. T. Poh, "Diagnosis of virus infection in orchid plants with high-resolution optical coherence tomography," *Journal of biomedical optics*, vol. 14, pp. 014006-014006-6, 2009.

[34] N. K. Ravichandran, R. E. Wijesinghe, M. F. Shirazi, K. Park, S.-Y. Lee, H.-Y. Jung, M. Jeon, and J. Kim, "In vivo monitoring on growth and spread of gray leaf spot disease in Capsicum annuum leaf using spectral domain optical coherence tomography," *Journal of Spectroscopy*, vol. 2016, 2016.

[35] R. Wijesinghe, S.-Y. Lee, N. K. Ravichandran, M. F. Shirazi, and P. Kim, "Optical screening of Venturianashicola caused Pyruspyrifolia (Asian pear) scab using optical coherence tomography," *International Journal of Applied Engineering Research*, vol. 11, pp. 7728-7731, 2016.

[36] R. E. Wijesinghe, S.-Y. Lee, P. Kim, H.-Y. Jung, M. Jeon, and J. Kim, "Optical sensing method to analyze germination rate of Capsicum annum seeds treated with growth-promoting chemical compounds using optical coherence tomography," *Journal of Biomedical Optics*, vol. 22, pp. 091502-091502, 2017.

[37] M. Jeon, J. Kim, U. Jung, C. Lee, W. Jung, and S. A. Boppart, "Full-range k-domain linearization in spectral-domain optical coherence tomography," *Applied optics*, vol. 50, pp. 1158-1163, 2011.